Escherichia coli NusG links the lead ribosome with the transcription elongation complex

Robert S. Washburn[1], Philipp K. Zuber[2], Ming Sun[3,4], Yaser Hashem[5,6], Bingxin Shen[5,7], Wen Li[5], Sho Harvey[8,9], Stefan H. Knauer[2,*], Joachim Frank[3,5,*], and Max E. Gottesman[1,5,*]

[1]Department of Microbiology & Immunology, Columbia University Medical Center, New York, NY 10032, USA.

[2]Biopolymers, University of Bayreuth, Universitaetsstrasse 30, 95447 Bayreuth, Germany.

[3]Department of Biological Sciences, Columbia University, New York, NY 10027, USA.

[4]Current address: University of California at San Francisco, San Francisco, CA 94158, USA.

[5]Department of Biochemistry and Molecular Biophysics, Columbia University Medical Center, New York, NY 10032, USA.

[6]Current address: NSERM U1212, Institut Européen de Chimie et Biologie, University of Bordeaux, Pessac 33607, France.

[7]Current address: Bristol-Myers Squibb Pharmaceutical Co., New Brunswick, NJ 08901, USA.

[8]University of Michigan, Ann Arbor, MI 48109, USA.

[9]Current address: California Institute of Technology, Pasadena, CA 91125, USA.

*Corresponding Authors

Abstract

It has been known for more than 50 years that transcription and translation are physically coupled in bacteria, but whether or not this coupling may be mediated by the two-domain protein N-utilization substance (Nus) G in *Escherichia coli* is still heavily debated. Here, we combine integrative structural biology and functional analyses to provide conclusive evidence that NusG can physically link transcription with translation by contacting both RNA polymerase and the ribosome. We present a cryo-electron microscopy structure of a NusG:70S ribosome complex and nuclear magnetic resonance spectroscopy data revealing simultaneous binding of NusG to RNAP and the intact 70S ribosome, providing the first direct structural evidence for NusG-mediated coupling. Furthermore, *in vivo* reporter assays show that recruitment of NusG occurs late in transcription and strongly depends on translation. Thus, our data suggest that coupling occurs initially via direct RNAP:ribosome contacts and is then mediated by NusG.

Introduction

Gene expression is a universal process in all cells and consists of transcription, i.e. the synthesis of RNA based on the DNA, and – if RNA is not the final gene product – translation, i.e. the messenger RNA (mRNA)-guided synthesis of a protein. Since the late 1960s it has been known that the rates of transcription and translation are synchronized in *Echerichia coli* so that mRNA is translated while being transcribed (Das et al., 1967; Mehdi and Yudkin, 1967; Miller et al., 1970; Proshkin et al., 2010; Vogel and Jensen, 1994, 1995). This process,called transcription:translation coupling, is possible due to the lack of a physical barrier between transcription and translation in bacteria (reviewed in (Conn et al., 2019)). Only recently, direct physical interactions between RNA polymerase (RNAP) and the ribosomes have been demonstrated (Demo et al., 2017; Fan et al., 2017; Kohler et al., 2017), consistent with earlier observations that transcriptional events may control translation activity and *vice versa*(Proshkin et al., 2010). As transcription and translation are closely connected to other central processes in a bacterial cell, such as DNA repair (Pani and Nudler, 2017) and protein folding (Thommen et al., 2017), transcription:translation coupling constitutes one of the key resulatory functions in bacterial gene expression.

However, there are also indications that transcription:translation coupling may involve a member of the family of N-utilization substance (Nus) G proteins, which serves as adapter connecting RNAP and the lead ribosome (Burmann et al., 2010, 2012; Saxena et al., 2018; Zuber et al., 2019). *E. coli* Nus G, member and eponym of the only universally conserved class of transcription factors (Werner, 2012), consists of two

62 domain, an N- and a C-terminal domain (NTD and CTD, resepectively) connected v*ia* a
63 flexible linker, which move independently (Burmann et al., 2011; Mooney et al., 2009a).
64 NusG-NTD binds RNAP and accelerates transcription elongation (Burova et al., 1995;
65 Kang et al., 2018; Mooney et al., 2009a). Structural studies demonstrate that NusG-CTD,
66 which is a five-stranded β-barrel with a Kyrpides-Ouzounis-Woese motif (Kyrpides et al.,
67 1996), is a versatile binding platform for different transcription factors. By binding to
68 protein S10, which is part of the 30S subunit of the ribosome, NusG may link
69 transcription and translation (Burmann et al., 2010). Saxena *et al* also demonstrated
70 specific 1:1 binding of NusG to 70S ribosomes both *in vitro* and *in vivo* (Saxena et al.,
71 2018).

72 S10 is identical with transcription factor NusE and forms a ribosome-free
73 complex with NusB, NusA and NusG which suppresses transcription termination
74 (Dudenhoeffer et al., 2019; Krupp et al., 2019; Said et al., 2017; Squires et al., 1993).
75 Finally, NusG-CTD binds to termination factor Rho and is required for most Rho activity
76 *in vivo* (Burmann et al., 2010; Lawson et al., 2018; Mitra et al., 2017).
77 Transcription:translation coupling prevents Rho factor from terminating transcription by
78 sequestering the NusG-CTD and by blocking Rho access to RNAP via untranslated
79 mRNA. Cryptic *E. coli* Rho-dependent terminators located within open reading frames
80 (orfs) are revealed when ribosomes are released by polar nonsense mutations (Cardinale
81 et al., 2008; Newton et al., 1965).

82 Nevertheless, there is evidence for intragenic uncoupling and Rho-dependent
83 transcription termination in the absence of nonsense mutations. Washburn and
84 Gottesman (Washburn and Gottesman, 2011) and Dutta et al. (Dutta et al., 2011) found

that Rho resolves clashes between transcription and replication. Such conflicts are likely to occur within, rather than at the end of, genes. Uncoupling would allow Rho to release the stationary transcription elongation complexes (TECs).

Mutations in *nusE* or *nusG* that uncouple transcription from translation increase sensitivity to chloramphenicol (Saxena et al., 2018). This antibiotic retards translation, breaking the bond between the lead ribosome and TEC. Uncoupled TEC may backtrack or terminate prematurely (Dutta et al., 2011).

In this report, we present a cryo-electron microscopy (cryo-EM) structure showing NusG binding to the S10 subunit in a 70S ribosome. The NusG-CTD binding site of S10 is also target of the ribosome-release factor, transfer-messenger (tmRNA), raising the possibility that tmRNA might displace NusG at rare codons, thereby uncoupling transcription from translation (Roche and Sauer, 1999). We also show by solution-state nuclear magnetic resonance (NMR) spectroscopy that NusG, once bound to RNAP, can interact with S10 or with a complete ribosome, setting the structural basis for coupling.

NusG couples transcription with translation *in vivo*, as proposed earlier (Burmann et al., 2010). Uncoupling of RNAP from the lead ribosome is enhanced when translation is compromised. Importantly, we demonstrate that uncoupled RNAP can outpace translation, leading to Rho-dependent transcription termination. This intragenic termination explains the necessity for the apparent perfect synchronization between transcription and translation (Proshkin et al., 2010).

Results

Structural evidence of NusG binding to the ribosomal S10 subunit on a 70S ribosome.

We assembled a NusG:70S complex by incubating 70S ribosomes with an excess of NusG and determined the structure of this complex by cryo-EM and single-particle reconstruction. Overall, 188,127 particles were extracted from 1327 images and ~5% of these particles showed an extra mass of density attached to the mass identified as protein S10 (Fig. 1A,B). This additional density perfectly matches the size of NusG-CTD, suggesting that NusG binds at the site predicted from the solution NMR structure of NusG-CTD bound to the free ribosomal protein S10 in a 1:1 stoichiometry (Fig. 1A,B; (Burmann et al., 2010)). The density map reconstructed from the class of NusG:70S particles was refined to an average resolution of 6.8 Å. No density could be observed for NusG-NTD, indicating that it is flexibly bound to the NusG-CTD and does not interact with the ribosome.

During translation ribosomes may stall on incomplete mRNAs, i.e. they reach the 3' end of an mRNA without terminating, resulting in an unproductive translation complex. Together with the small protein B (SmpB) tmRNA can bind to these stalled ribosomes in order to rescue them and to tag the nascent polypeptide chain for degradation in a process called trans-translation (Weis et al., 2010). Interestingly, the NusG-CTD binding site overlaps with the region of S10 that is contacted by the tmRNA when it is bound to a ribosome in its resume state (Fig. 1C; (Burmann et al., 2010; Fu et al., 2010; Rae et al., 2019; Weis et al., 2010)). From this we conclude that NusG-CTD and tmRNA share binding sites on S10, raising the possibility that, in addition to

130 releasing stalled ribosomes, tmRNA competes with NusG for ribosome binding, thus
131 preventing NusG from maintaining a linkage between the lead ribosome and RNAP. In
132 other words, tmRNA might be able to displace NusG and thereby facilitate uncoupled
133 transcription.
134
135 **Simultaneous binding of NusG to S10 and RNAP**
136 In the cryo-EM structure of *E. coli* NusG bound to a paused TEC (Kang et al., 2018) only
137 the density of NusG-NTD was observable, indicating that NusG-CTD moves freely and
138 does not interact with RNAP. Binding of NusG-CTD to S10 was observed both in a
139 binary system (Burmann et al., 2010) and a λN-dependent antitermination complex
140 (Krupp et al., 2019; Said et al., 2017).
141 Since the NusG-CTD:S10 interaction is a prerequisite for NusG-mediated
142 transcription:translation coupling, we probed this contact when NusG was bound to
143 RNAP - but not in an antitermination context - by solution-state NMR spectroscopy. We
144 employed NusG samples where [^{1}H,^{13}C]-labeled methyl groups of Ile, Leu, and Val
145 residues in perdeuterated proteins served as NMR-active probes ([ILV]-NusG) to
146 increase sensitivity, allowing us to study large systems.
147 In the methyl-transverse relaxation optimized spectroscopy (methyl-TROSY)
148 spectrum of free [ILV]-NusG (Fig. 2A), signals of the NusG-NTD and NusG-CTD
149 perfectly superimpose with the signals of the isolated [ILV]-labeled protein domains,
150 suggesting that the domains move independently, confirming a previous report stating
151 that there are no intramolecular domain interactions (Burmann et al., 2011). Upon
152 addition of RNAP in a two-fold molar excess, [ILV]-NusG signals were significantly

153 decreased in the one-dimensional methyl-TROSY spectrum (Fig. 2B, inset), indicating
154 [ILV]-NusG:RNAP complex formation. Binding of RNAP increases the molecular mass
155 of [ILV]-NusG dramatically, resulting in enhanced relaxation, which ultimately leads to
156 drastic line broadening and a decrease in signal intensity. Interestingly, the two-
157 dimensional spectra revealed a non-uniform signal decrease (Fig. 2B), which is caused by
158 a combination of several effects. First, there is a general loss of signal intensity due to the
159 increase in molecular mass upon complex formation, as discussed above. Second, upon
160 binding, methyl groups of Ile, Leu, and Val residues located in the binding surface come
161 into close proximity of RNAP protons. Dipole-dipole interactions contribute to relaxation
162 processes so that the signal intensity of these methyl groups is decreased more strongly
163 than that of methyl groups located elsewhere in [ILV]-NusG. Finally, signal intensities
164 may be affected by chemical exchange processes. We analyzed the signal intensity of
165 [ILV]-NusG signals in the presence of RNAP quantitatively by calculating relative signal
166 intensities, i.e. the ratio of the remaining signal intensity of [ILV]-NusG in the presence
167 of RNAP to the signal intensity of free [ILV]-NusG (Figure 2-figure supplement 1).

168 The average relative intensity of NusG-NTD signals was significantly lower than
169 that of the linker or the NusG-CTD, suggesting that NusG-NTD binds to RNAP whereas
170 NusG-CTD remains flexible and moves independently, able to interact with other
171 partners, as indicated by the NusG:TEC structure (Kang et al., 2018). The signal intensity
172 of all Ile, Leu, and Val residues in the RNAP binding site of NusG was completely
173 extinguished, confirming that NusG-NTD binds to RNAP at its known binding site
174 (Drögemüller et al., 2015; Kang et al., 2018; Krupp et al., 2019; Said et al., 2017).

To test if NusG-CTD can bind to S10 while being tethered to RNAP *via* NusG-NTD, we titrated the [ILV]-NusG:RNAP complex with $S10^{\Delta}$ (Fig. 2C). In order to increase stability, we used this S10 variant lacking the ribosome binding loop in complex with NusB (Luo et al., 2008). Chemical shift changes of [ILV]-NusG-CTD signals upon titration of [ILV]-NusG:RNAP with $S10^{\Delta}$:NusB were determined (Fig. 2D) and affected residues were mapped onto the three-dimensional structure of NusG-CTD (Fig. 2E). Strongly affected residues are found to be located in β-strands 3 and 4 as well as in the connecting loop, in agreement with the binding site observed in the binary NusG-CTD:$S10^{\Delta}$ complex (Burmann et al., 2010). The loop between β-strands 1 and 2 is also part of the NusG-CTD:$S10^{\Delta}$ binding site, but as it does not contain any Ile, Leu, or Val residues, no NMR-active probes are available in this region; nevertheless, affected residues can be found in β-strand 1, directly preceding this loop. This suggests that the CTD:$S10^{\Delta}$ binding surface in the RNAP:NusG:$S10^{\Delta}$:NusB complex is identical to the one determined in the binary system. Importantly, the NusG-NTD signals do not change when S10 is added to the NusG:RNAP complex, indicating that S10 binding does not release the bound RNAP.

We conclude that the S10 interaction site of NusG-CTD is accessible in the NusG:RNAP complex and thus can promote ribosome binding and formation of a ribosome:NusG:RNAP complex.

To look for a ribosome:NusG-RNAP complex, we repeated the experiment using intact 70S ribosomes instead of $S10^{\Delta}$:NusB (Figure 3). In a first test, we titrated [ILV]-NusG with 70S ribosomes (Figure 3A). As in the [ILV]-NusG:RNAP experiment, signal

198 intensity of [ILV]-NusG methyl groups was significantly, but not uniformly, decreased.
199 In the presence of a twofold molar excess of ribosomes some NusG-NTD signals
200 remained visible, whereas most NusG-CTD signals were nearly completely extinguished.
201 Quantitative analysis of the [ILV]-NusG methyl group signal intensity in the presence of
202 0.5 equivalents of 70S ribosomes clearly shows that the relative intensity of NusG-CTD
203 signals was in a narrow range < 2 %, whereas the relative intensity of NusG-NTD signals
204 covered values from 0-4 %, and was higher on average (Figure 3B). Relative intensities
205 of zero of NusG-NTD signals can be attributed to the fact that these signals are weak
206 even in free NusG, and can thus not be quantified upon ribosome binding. Due to the
207 flexibility of the linker, signals corresponding to amino acids in this region had the
208 highest relative signal intensities. From these results we conclude that NusG binds to the
209 ribosome via its CTD, in agreement with our cryo-EM structure (Figure 1). Due to the
210 drastic increase in molecular mass we were unable to determine a binding site from these
211 experiments, but nevertheless, the pattern of intensity changes of NusG-CTD signals was
212 similar to that resulting form the titration of RNAP-bound NusG with S10, i.e. the most
213 drastic decrease of signal intensity can be observed for residues 160-170, which are part
214 of β-strands 3 and 4 and the intervening loop. Consequently, we conclude that the
215 ribosome binding site is identical with the binding site for isolated S10.

216 Next, we formed a complex of [ILV]-NusG and RNAP (molar ratio 1:2). The 2D
217 methyl-TROSY spectrum of the complex revealed a decrease of signal intensities typical
218 for NusG binding to RNAP (see Fig. 2C), i.e. primarily NusG-CTD signals remained
219 visible. When we then added one equivalent of 70S ribosomes nearly all [ILV]-NusG
220 signals were diminished (e.g. the signal corresponding to I164, which is in the loop

221 responsible for ribosome binding). Strikingly, the spectrum differs from the spectrum of
222 [ILV]-NusG in the presence of 70S ribosome (Fig. 3A). These results can be explained
223 by three scenarios: (i) NusG-NTD is bound to RNAP, NusG-CTD is bound to a
224 ribosome, and the ribosome directly interacts with RNAP, (ii) NusG-NTD is bound to
225 RNAP, NusG-CTD is bound to the ribosome, but the ribosome does not interact with
226 RNAP, (iii) NusG-NTD is bound to RNAP, the ribosome directly interacts with RNAP,
227 and NusG-CTD is free, but is in the vicinity of the ribosome. To exclude the last scenario
228 we repeated the experiment using a NusG variant, NusG^{F165A}, in which F165, essential
229 for ribosome binding (Burmann et al., 2010; Knowlton et al., 2003), is substituted by an
230 Ala. Having ensured that the amino acid substitution does not influence the structure of
231 NusG (Fig. 3-figure supplement 1A) we tested in a control experiment [ILV]-NusG^{F165A}
232 binding to S10^{A}. Indeed, we could detect no interaction (Fig. 3-figure supplement 1B,C).
233 When we added 70S ribosomes to a preformed [ILV]-NusG^{F165A}:RNAP complex (molar
234 ratio 2:1), the spectrum corresponding to the [ILV]-NusG^{F165A}:RNAP complex did not
235 significantly change and, in particular, NusG-CTD signals remained visible, suggesting
236 that the ribosome was not bound. However the general decrease in signal intensity
237 indicated a direct RNAP:ribosome interaction. Thus, we conclude that NusG can serve as
238 physical linker between ribosome and RNAP, although it remains elusive if a direct
239 interaction between RNAP and a ribosome occurs in this NusG-coupled complex.
240
241 **Translation promotes NusG attachment to TEC.**
242 Chromatin Immuno Precipitation (ChIP) analysis showed that NusG binds to TEC well
243 after transcription and translation initiation (Mooney et al., 2009b). Thus, we asked

whether translation was, in fact, required for attachment of NusG to TEC. To approach this question, we examined the effects of translation on NusG-mediated Rho-dependent termination within the *lac* operon (Fig. 4A, Table 1) as NusG recruitment to the TEC is necessary for efficient Rho-dependent termination. Rho-dependent termination occurs within *lacZ* both *in vitro* (Burns and Richardson, 1995) and, upon the introduction of *lacZ* nonsense mutations, *in vivo* (Adhya and Gottesman, 1978; Newton et al., 1965). Polarity was measured using a probe to *lacA*, comparing mRNA levels with or without treatment with the Rho inhibitor bicyclomycin (BCM). Wildtype (WT) cells revealed no detectable termination (Table 1, Fig. 4A-I), which may be attributed to (i) sequestering of NusG-CTD by the ribosome, (ii) binding of the ribosome to the nascent RNA, or (iii) both. In all scenarios, however, the presence of the translating ribosome prevents Rho binding. We interfered with translation initiation by mutating the ribosome-binding site, i.e. the Shine-Dalgarno (SD) sequence (Fig. 4A-II), or translation elongation by introducing six successive rare arginine codons at two different locations in *lacZ* (Fig. 4A III, IV). Introduction of two G to A mutations in the *lacZ* SD sequence prohibits translation initiation of *lacZ* (Fig. 4A-II). *lacA* mRNA measurements gave a read-through of 21%, indicating that Rho-dependent termination occurs, but was inefficient in the absence of translation of *lacZ* mRNA. Introduction of the six in-frame rare arginine residues at the +4 position of *lacZ* (Fig. 4A-III, Table 1) allowed 29% read-through, i.e. Rho-dependent termination is present, but still inefficient if translation of *lacZ* mRNA is interfered with at early elongation. In contrast, introduction of the rare arginine residues 200 nt from the start site of transcription (Fig. 4A-IV, Table 1) resulted in high polarity, yielding < 1 %

read-through. As efficient Rho-dependent termination requires NusG our results suggests that NusG binding to TEC occurs late and is dependent on translation.

To confirm the hypothesis that NusG failed to attach to TEC in the absence of translation, we asked if a complex comprising Nus factors A, B, and E (Nus complex) assembled at a λ *nutL* site was able to recruit NusG so that it associates with TEC. Accordingly, we introduced the λ *nutL* site just upstream of the flawed *lacZ* SD sequence and measured *lacA* mRNA (Figure 4B, Table 1). Indeed, Rho-dependent termination was highly efficient, indicating that NusG had been recruited to TEC. Thus, counterintuitively, the Nus complex, which normally suppresses transcription termination in ribosomal (*rrn*) operons and, together with λN, on the phage λ chromosome, stimulates termination in this case.

We finally demonstrated that reduced termination efficiency in the mutant with the non-functional SD sequence was due to the failure of NusG recruitment to the TEC. In this assay we monitored Rho-dependent termination in a fusion construct that carries λ *cro,* the λ *nutR* site, the Rho-dependent λ *tR1* terminator and a *lacZ* reporter, with *lacZ* expression being heat-inducible (Fig. 5). Termination at the λ *tR1* site is poor when *cro* is translated, as seen with the *cro ms27* fusion (Table 2A, Fig. 5A-I; in the presence of an intact SD sequence we used *cro ms27*, where codon 27 carries a missense mutation so that the resulting protein is non-functional). The 3' end of *cro* is adjacent to the λ *tR1* terminator, limiting the amount of free RNA available for Rho attachment if *cro* mRNA is translated. When λ *cro* carried a SD mutation translation initiation was ablated, but nevertheless there was significant termination at λ *tR1* (Table 2A, Figure 5A-II, compare read-through values with and without BCM). Formation of the Nus complex at λ *nutR*

289 allows NusG recruitment and efficient termination. In the absence of NusB, the complex
290 does not assemble, and there is extensive read-through at λ *tR1*.

291 The *boxA69* mutation also reduces Nus complex formation at λ *nutR*, and like the
292 *nusB*- mutation, enhances read-through of λ *tR1* (Table 2B, Fig. 5B). In this experiment,
293 we suppressed termination at λ *tR1* with λ N antitermination factor instead of BCM.
294 Finally, we showed that expression of *nusG-NTD*, which competes with NusG for
295 binding to RNAP, enhances read-through (Table 2C, Fig. 5C). Taken together, these
296 results strongly support the idea that NusG can be supplied by the Nus complex
297 assembled at λ *nutR* in the absence of translation, inducing Rho-dependent termination at
298 λ *tR1*.
299

Discussion

We determined a cryo-EM structure of a NusG: 70S complex showing binding of one molecule NusG per ribosome, consistent with previous results (Saxena et al., 2018). NusG binds to the S10 protein on the 30S subunit via its CTD as indicated by the study of isolated NusG-CTD and S10 (Burmann et al., 2010); density for NusG-NTD was not observable, suggesting that it remains flexible. We must attribute the low occupancy of the NusG-CTD on the 70S ribosome in the cryo-EM experiment to weak binding adversely affected by the conditions of sample preparation. Notably, although tmRNA contacts the ribosome at various sites, the binding of NusG-CTD and tmRNA on S10 is mutually exclusive. This suggests a model in which uncoupling at rare codons, at which tmRNA releases ribosomes, is promoted by tmRNA-induced release of NusG (Roche and Sauer, 1999). The freed NusG:TEC complex exposes the NusG-CTD, and is then subject to Rho-dependent transcription termination.

Simultaneous binding of NusG to S10 and RNAP has been demonstrated by solution-state NMR studies, confirming the S10 binding site on NusG-CTD as identified in a binary NusG-CTD:S10 system (Fig. 2) (Burmann et al., 2010). Moreover, we show that NusG can bind RNAP and 70S ribosome simultaneously; this is the first direct structural evidence for NusG-mediated transcription:translation coupling. The flexibility of the linker between the NusG-NTD and the NusG-CTD permits these interactions. The operon-specific *E. coli* NusG paralog, RfaH, likewise simultaneously binds S10 and RNAP in the context of a paused TEC (Burmann et al., 2012; Zuber et al., 2019). RfaH, which also comprises an NTD and a flexibly-connected CTD (Belogurov et al., 2007; Burmann et al., 2012), uses the same binding sites as NusG to interact with RNAP and

S10 (Burmann et al., 2010, 2012; Kang et al., 2018; Sevostyanova et al., 2011; Zuber et al., 2019). However, RfaH, unlike NusG, complexes with TEC early after transcription initiation, when TEC pauses at an operon polarity suppressor (*ops*) site, a representative of the *E. coli* consensus pause sequence (Larson et al., 2014; Vvedenskaya et al., 2014). Located in the untranslated leader region of RfaH-controlled operons, *ops* is responsible for sequence-specific recruitment of RfaH (Zuber et al., 2018). Importantly, RfaH-dependent operons lack a consensus SD sequence . To initiate translation, RfaH recruits a ribosome to these mRNAs, making coupling essential for translation activation and efficient gene expression (Burmann et al., 2012). The binding modes of RfaH and NusG to RNAP and S10 are very similar, indicating that coupling as observed for RfaH can also be mediated by NusG and vice versa. However, once recruited, RfaH excludes NusG (Kang et al., 2018), thus preventing intra-operon Rho-dependent transcription termination in RfaH-controlled operons (see (Artsimovitch and Knauer, 2019)).

We have confirmed the results of Mooney et al that NusG binds to TEC only after significant RNA synthesis (Mooney et al., 2009b). As postulated by these authors, binding depends on active translation of the mRNA. Thus efficient Rho-dependent transcription termination, which requires the attachment of Rho to the NusG-CTD, does not occur at the end of an untranslated gene. We have shown that the failure of NusG to bind TEC is responsible for the absence of termination. Thus, placing a λ *nut* site at the start of the gene recruits NusG and restores termination. At present, it is not understood why NusG appears to be delivered to TEC by ribosomes *in vivo*, whereas it binds directly to RNAP in a purified system lacking ribosomes. A possible explanation would be that NusG binds to RNAP discontinuously in an on-and-off mode in the untranslated leader

region and that the NusG:RNAP interaction is only stabilized when the ribosome is coupled upon translation initiation. We should recall that NusG has two binding sites in the coupled system, which significantly increases its affinity.

A direct connection between transcription and translation was first predicted in 1964 (Byrne et al., 1964). Transcription:translation coupling is necessary to coordinate gene expression and to maintain genome stability (McGary and Nudler, 2013). In 1970, Miller *et al.* performed electron miscroscopy analyses of lysed *E. coli* cells (Miller et al., 1970). They demonstrated that all mRNA molecules are connected to the *E. coli* genome, and that the ribosome at the newly synthesized end of a polyribosome is almost always immediately adjacent to the putative RNAP molecule. They concluded that translation is completely coupled with transcription. Coupling could allow RNAP to monitor the translation rate while providing newly synthesized mRNA to the ribosome. The structural basis of this coupling is, however, still only poorly understood. Our results strongly suggest that NusG may mediate coupling. However, since NusG attaches to the TEC downstream to the translation initiation site, the coupled transcription:translation complex must initially consist of a ribosome bound directly to TEC, in agreement with two cryo-EM structures and *in vitro* data (Demo et al., 2017; Fan et al., 2017; Kohler et al., 2017). One cryo-EM structure shows the so-called "expressome", an RNAP:70S complex generated by letting a ribosome translate until it encounters a stalled RNAP (Fig. 6A; (Kohler et al., 2017)). In this complex RNAP directly binds to the 30S subunit with the RNA exit region of RNAP docking onto the ribosome near the mRNA tunnel entry between ribosomal proteins S3, S4, and S5. In this structure, mRNA exiting from RNAP can directly enter the ribosome. Another cryo-EM structure showed an RNAP:30S

complex generated by mixing 30S subunit with a 3-fold excess of RNAP (Fig. 6B; (Demo et al., 2017)). In this structure RNAP is bound to the 30S subunit near the mRNA binding site between the head and the platform domains, contacting ribosomal proteins S1, S2, S18, S21, and hairpin loop 40 of 16S rRNA, in agreement with crosslinking data (Fan et al., 2017). Strikingly, this position is located more than 80 Å from the binding site observed in the expressome structure, i.e. on the opposite side of the 30S head. Importantly, it ensures that RNAP interacts with the cytosolic site of the 30S ribosomal subunit so that the nascent RNA exiting from RNAP is directly guided to the entry site on the ribosome. Assuming that the RNAP:30S complex corresponds to a coupling complex at translation initiation and the expressome structure to a translation elongation complex, a would require a massive relocalization of RNAP.

Interestingly, neither the RNAP:30S nor the expressome structures allow NusG- (or RfaH-) mediated coupling: the linker of NusG/RfaH is too short (Fig. 6). However, as the cryo-EM structures suggest that the position of RNAP on the 30S subunit might be flexible, these structures could be snapshots of distinct situation during translation. Thus, we suggest that at some distance downstream of the translation initiation site, NusG recognizes and enters the coupling complex.

In summary, we hypothesize that two coupling modes exist, a direct coupling between the ribosome and TEC during translation initiation and early elongation and a NusG-mediated coupling mode later in translation. The question of whether the 70S ribosome still directly contacts TEC in the NusG-mediated system remains elusive. The expressome structure (Kohler et al., 2017) does not allow simultaneous NusG binding to TEC and the 70S ribosome, thus the relative orientation of 70S ribosome to TEC might

392 be different in the direct and the NusG-mediated system. The latter may thus require a
393 reorientation of the TEC and the 70S ribosome and confer the system more flexibility,
394 necessary to keep transcription and translation synchronized, even if these processes are
395 differently regulated or occur at different rates.
396

Methods

Strain Construction. Standard bacteriological techniques used in strain construction (e.g., transformation, transduction and media preparation) are as described in Silhavy et al. (1984). Standard molecular biology techniques were as described in Sambrook and Russell (Sambrook and Russel, 2001). N10780 was constructed by P1 transduction of *rpoC-his:kanR nusGF165A* from NB885 into MDS42. N11158 was constructed by P1 transduction of Δ*ssrA::camR* from RSW943 into MDS42. N11816 was constructed by P1 transduction of Δ*relA::kanR* from RLG847 into N11158. RSW1008 was constructed by P1 transduction of Δ*ssrA::camR* from RSW943 into N4837. RSW1010 was constructed by P1 transduction of *rpoC-his:kanR nusGF165A* from NB885 into N4837. RSW1012 was constructed by P1 transduction of Δ*ssrA::camR* from RSW943 into RSW1010. RSW1175 was constructed by P1 transduction of *ΔrelA::kanR* and *ΔspoT::camR* from RLG847 into MDS42. RSW1245 was generated using recombineering (Sharan et al., 2009) to introduce six rare arginine codons (atg-acc-atg-AGG-AGA-CGA-AGG-AGA-CGA-att-acg-gat) into the 5'end of *lacZ* in MDS42 changing the amino acid sequence of the aminoterminus from MTMITD to MTMRRRRRRITD with six inefficiently translated arginine codons. RSW1225 was produced using recombineering to introduce two G to A mutations in the ribosome binding site of *lacZ* in MDS42. This resulted in a change from …TTCACACAGGAAACAGCTatgaccatg… to …TTCACACACC AAACAGCTatgaccatg…inactivating the ribosome binding site. RSW1225 is *lac*$^{-}$.

Cloning. The plasmid encoding NusG-F165A was generated by site-directed mutagenesis according to the QuikChange Site-Directed Mutagenesis Kit (Stratagene), using vector pET11A_*nusG* (Burmann et al., 2011) as template and primers Fw_NusG-F165A (5' GTG TCT GTT TCT ATC GCG GGT CGT GCG ACC CCG 3') and Rv_NusG-F165A (5' CGG GGT CGC ACG ACC CGC GAT AGA AAC AGA CAC 3'; both primers were obtained from metabion, Martinsried, Germany).

Protein production and isotopic labeling. NusG and NusG-NTD were produced as described (Burmann et al., 2011) as were NusG-CTD (Burmann et al., 2010) and RNAP and $S10^{\lambda}$:NusB used for NMR spectroscopy (Zuber et al., 2019). Production of NusG-F165A was analogous to NusG (Burmann et al., 2011). For unlabeled proteins, bacteria were grown in lysogeny broth (LB) medium. [^{1}H,^{13}C]-labeling of methyl groups of Ile, Leu, and Val residues in perdeuterated proteins was accomplished by growing bacteria in M9 medium (Meyer and Schlegel, 1983; Sambrook and Russel, 2001) prepared with increasing amounts of D_2O (0 % (v/v), 50 % (v/v), 100 % (v/v); Eurisotop, Saint-Aubin, France) and $(^{15}NH_4)_2SO_4$ (CortecNet, Voisins-Le-Bretonneux, France) and d_7-glucose (Cambridge Isotope Laboratories, Inc., Tewksburgy, USA) as sole nitrogen and carbon sources, respectively. Amino acid precursors (60 mg/l 2-keto-3-d_3-4-^{13}C-butyrate and 100 mg/l 2-keto-3-methyl-d_3-3-d_1-4-^{13}C-butyrate; Eurisotop, Saint-Aubin, France) were added 1 h prior to induction. Expression and purification protocols were identical to those of the non-labeled proteins.

441 Intact 70S ribosomes were produced as follows. *E. coli* strain MRE600 cells grown in LB
442 medium were harvested, lysed by passing through the French Press 3x at ~800 PSI, and
443 clarified by a short centrifugation (20,000 rpm, 40min) in opening buffer (20 mM Tris-
444 HCl pH=7.5, 100mM NH_4Cl, 10.5 mM Mg acetate, 0.5 mM EDTA, with half a protease
445 inhibitor cocktail tablet (Roche, EDTA-free), and 1mM TCEP added just before use). The
446 lysate was loaded onto the top of 5 mL sucrose cushion (20 mM Tris-HCl, pH=7.5, 500
447 mM NH_4Cl, 10.5 mM Mg acetate, 0.5 mM EDTA, 1.1 M sucrose, and 1 mM TCEP
448 added before use) and centrifuged for 24 h at 28,000 rpm in a 70Ti rotor (Beckman
449 Coulter, Inc.). The pellets were suspended in washing buffer (20 mM Tris-HCl, pH=7.5;
450 500mM NH_4Cl, 10.5mM Mg acetate, 0.5mM EDTA and 1 mM TCEP added before use),
451 and centrifuged through a 10–35% sucrose gradient for 19 h at 16,000 rpm in a SW28
452 rotor (Beckman Coulter, Inc.). Fractions containing the 70S peaks were pooled and kept
453 at -80℃ for further use.
454 Ribosomes for NMR experiments were obtained from New England Biolabs.
455

456 **Electron Microscopy**

457 Purified 70S ribosomes were incubated with full-length NusG at a ratio of 1:7 for 40 min
458 at room temperature, prior to blotting and plunge-freezing as previously described
459 (Grassucci et al., 2007). Data were collected on a TF30 Polara electron microscope (FEI,
460 Portland, Oregon) at 300kV using a K2 Summit direct electron detector camera (Gatan,
461 Pleasanton, CA). Images were recorded using the automated data collection system
462 Leginon (Suloway et al., 2005) in counting mode, and taken at the nominal magnification
463 of 32,000x, corresponding to a calibrated pixel size of 1.66Å.

464 **Image processing**

465 A total of 188,127 particles were automatically extracted from 1327 images using
466 Arachnid (Langlois et al., 2014). RELION (Scheres, 2012) 3D classification was used to
467 resolve the heterogeneity of the particle images, and auto-refinement to further improve
468 resolution for each class. The final refinement for the NusG-bound 70S class containing
469 17,122 particles yielded an average resolution of ~6.8Å (FSC=0.143; following "gold
470 standard" protocol).

471

472 **Model building**

473 The starting model was assembled from the X-ray structure of the *E. coli* 30S ribosomal
474 subunit (PDB ID 4GD2) and the NMR solution structure of the NusG-CTD (PDB 2KVQ
475 chain G). This starting model was first docked into the segmented maps of our 70S
476 density map as a rigid body using UCSF Chimera (Pettersen et al., 2004). Then it was
477 fitted into the segmented map using the Molecular Dynamic Flexibly Fitting (MDFF)
478 method (Trabuco et al., 2008) and run using the NAMD program (Phillips et al., 2005) for
479 0.5 ns of simulation time, followed by 5,000 steps of energy minimization.

480

481 **NMR spectroscopy.** NMR experiments were conducted on Bruker Ascend Aeon 900 and
482 1000 MHz spectrometers equipped with cryogenically cooled, inverse triple resonance
483 probes at 298 K. NMR data was converted and processed using in-house software. 2D
484 correlation spectra were visualized and analyzed with NMRViewJ (One Moon Scientific,
485 Inc., Westfield, NJ, USA), 1D spectra were plotted using MatLab (The MathWorks, Inc.,

Version 9.2.0.538062). Resonance assignments for NusG methyl groups were taken from a previous study (Mooney et al., 2009a).

[ILV]-NusG-CTD was in 10 mM K-phosphate (pH 7.5), 50 mM KCl, 1 mM $MgCl_2$, 99.9 % (v/v) D_2O, [ILV]-NusG-NTD in 50 mM Na-phosphate (pH 7.5), 50 mM KCl, 0.3 mM EDTA, 5 % (v/v) d_7-glycerol, 0.01 % (w/v) NaN_3, 99.9 % D_2O. For the titration of [ILV]-NusG with RNAP and $S10^D$:NusB, all proteins were in 50 mM Na-phosphate (pH 7.5), 50 mM KCl, 0.3 mM EDTA, 99.9 % (v/v) D_2O and 5 mM $MgCl_2$ and 2 mM DTT were added to the NMR sample to increase the-long-term stability of RNAP. For all interaction studies involving ribosomes and for the titration of [ILV]-NusG-F165A with $S10^A$:NusB, all components were in 20 mM HEPES-KOH (pH 7.6), 10 mM Mg-acetate, 30 mM KCl, 7 mM β-mercaptoethanol, 10 % D_2O. The titration of [ILV]-NusG-F165A with $S10^A$:NusB was conducted in a 5 mm tube with an initial sample volume of 550 µl. All other measurements were carried out in 3 mm NMR tubes with an (initial) volume of 200 µl.

1D and 2D titration experiments were evaluated quantitatively by analyzing either changes in signal intensity or changes in chemical shifts. If chemical shift changes were in the fast regime on the chemical shift the normalized chemical shift perturbation ($\Delta\delta_{norm}$) was calculated according to equation 1.

$$\Delta\delta_{norm} = \sqrt{\left(\Delta\delta\ ^1H\right)^2 + \left[0.25\ \left(\Delta\delta^{13}C\right)\right]^2} \quad (1)$$

with Δδ being the resonance frequency difference between the initial and final state of the titration (i.e. [ILV]-NusG:RNAP:$S10^D$:NusB = 1:2:0:0 *vs*. 1:2:2:2) in ppm.

509 If the system was in slow or intermediate chemical exchange the signal intensities were
510 analyzed quantitatively. First, the intensity of each 1D spectrum or methyl group signal,
511 respectively, was normalized by the concentration of the [ILV]-labeled protein, the
512 receiver gain, the number of scans, and the length of the 90° ^{1}H pulse. Then the relative
513 intensity, i.e. the ratio of the normalized signal intensity of [ILV]-labeled protein in the
514 respective titration step to the normalized signal intensity of free [ILV]-labeled protein,
515 was calculated and plotted against the sequence of NusG or the NusG variant,
516 respectively.
517
518 q**RT-PCR.** Total RNA was extracted from cells grown in M9 medium supplemented
519 with casamino acids (0.2%) at 37^{0}C to mid-log phase (O.D. 600=0.3). Fold-increase of
520 the PCR product was determined using qRT-PCR. cDNA was synthesized using RNA
521 was extracted from logarithmically growing cultures ($O.D._{600}$=0.2-0.3) Where indicated,
522 cells were treated with BCM (100μg/ml) 1 min before induction with 1mM IPTG for
523 *lacZ*. Samples were removed (0.5ml) at the indicated times and total RNA extracted
524 RNA extracted using Qiagen RNeasy and Qiagen RNAprotect Bacteria Reagent (Qiagen,
525 Germantown, MD). cDNA was synthesized from the samples using High Capacity RNA
526 to cDNA kit (ThermoFisher, Waltham, MA). qRT-PCR reactions were performed using
527 Taqman Gene Expression Master Mix (Thermofisher, Waltham, MA) and Biorad DNA
528 Engine Opticon2 Real-Time Cycler (Bio-Rad Laboratories, Hercules, CA) and
529 PrimeTime qPCR probes (Integrated DNA Technologies, Coralville, IA). The *lacA*
530 transcript was probed with the following: probe:5'-/56-
531 FAM/CCACATGAC/ZEN/TTCCGATCCAGACGTT/3IABkFQ/-3'; primer1:5'-

ATACTACCCGCGCCAATAAC; primer2:5'-CCCTGTACACCATGAATTGAGA). The reference gene was *ompA*(probe:5'-/56-FAM/CAACAACAT/ZEN/CGGTGACGCACACAC /3IABkFQ/-3'; primer1:5'-TGACCGAAACGGTAGGAAAC; primer2:5'-ACGCGATCACTCCTGAAATC). The PCR was performed using the following conditions: 50 °C for 10 min., 95 °C for 2 min, followed by 40 cycles each of 95 °C for 15s, and 60 °C 1min. All reactions were performed in duplicate. Fold increases were calculated from measured C_t values using the $\Delta\Delta C_t$ method (Livak and Schmittgen, 2001). Values are the average of three or more independent experiments.

β–galactosidase assays. Cultures were grown in LB to early log phase (O.D. 600 =0.3) at 37 ^{0}C. Where indicated bicyclomycin (BCM) (100μg/ml) was added to inhibit Rho-dependent transcription termination prior to induction of *lacZ* with 1mm IPTG. Where indicated λN was expressed by incubation at 42 °C. Reactions were terminated 15 min. after induction. β-galactosidase was measured using a modification of the method of Miller (Zhang and Bremer, 1995). Readthrough was calculated from the ratio of β-galactosidase activity +/- BCM.

Author Contributions: R.W., Y.H., M.S., W.L., B.S. P.K.Z. and S.H. performed the experiments. J.F., Y.H., M.S., R.W. P.K.Z. S.H.K. and M.G. designed the experiments and interpreted the results. M.S. M.G. M.S. P.K.Z. S.H.K. and J.F. wrote the paper.

Acknowledgments: We gratefully acknowledge the help of D. Shapoval, M. Bubunenko, N. Costantino and D. Court. We have had numerous useful discussions with P. Roesch and his group, for which we are most indebted. Supported by HHMI and NIH R01 GM29169 (to J.F.), NIH R01 GM037219 (to M.G.) and the German Research Foundation grant Ro617/21-1 (to P.R.). S.H. was supported by an Amgen Fellowship.

Competing interests. We declare no competing interests.

References

Adhya, S., and Gottesman, M. (1978). Control of transcription termination. Annu. Rev. Biochem. 47, 967–996.

Artsimovitch, I., and Knauer, S.H. (2019). Ancient Transcription Factors in the News. MBio 10.

Belogurov, G.A., Vassylyeva, M.N., Svetlov, V., Klyuyev, S., Grishin, N.V., Vassylyev, D.G., and Artsimovitch, I. (2007). Structural basis for converting a general transcription factor into an operon-specific virulence regulator. Mol. Cell 26, 117–129.

Burmann, B.M., Schweimer, K., Luo, X., Wahl, M.C., Stitt, B.L., Gottesman, M.E., and Rösch, P. (2010). A NusE:NusG complex links transcription and translation. Science 328, 501–504.

Burmann, B.M., Scheckenhofer, U., Schweimer, K., and Rösch, P. (2011). Domain interactions of the transcription-translation coupling factor *Escherichia coli* NusG are intermolecular and transient. Biochem. J. 435, 783–789.

Burmann, B.M., Knauer, S.H., Sevostyanova, A., Schweimer, K., Mooney, R.A., Landick, R., Artsimovitch, I., and Rösch, P. (2012). An α helix to β barrel domain switch transforms the transcription factor RfaH into a translation factor. Cell 150, 291–303.

Burns, C.M., and Richardson, J.P. (1995). NusG is required to overcome a kinetic limitation to Rho function at an intragenic terminator. Proc. Natl. Acad. Sci. U.S.A. 92, 4738–4742.

581 Burova, E., Hung, S.C., Sagitov, V., Stitt, B.L., and Gottesman, M.E. (1995). *Escherichia*
582 *coli* NusG protein stimulates transcription elongation rates *in vivo* and *in vitro*. J.
583 Bacteriol. 177, 1388–1392.

584 Byrne, R., Levin, J.G., Bladen, H.A., and Nirenberg, M.W. (1964). The *in vitro* formation
585 of a DNA-ribosome complex. Proc. Natl. Acad. Sci. U.S.A. 52, 140–148.

586 Cardinale, C.J., Washburn, R.S., Tadigotla, V.R., Brown, L.M., Gottesman, M.E., and
587 Nudler, E. (2008). Termination factor Rho and its cofactors NusA and NusG silence
588 foreign DNA in *E. coli*. Science 320, 935–938.

589 Conn, A.B., Diggs, S., Tam, T.K., and Blaha, G.M. (2019). Two Old Dogs, One New
590 Trick: A Review of RNA Polymerase and Ribosome Interactions during Transcription-
591 Translation Coupling. Int J Mol Sci 20.

592 Das, H.K., Goldstein, A., and Lowney, L.I. (1967). Attachment of ribosomes to nascent
593 messenger RNA in *Escherichia coli*. J. Mol. Biol. 24, 231–245.

594 Demo, G., Rasouly, A., Vasilyev, N., Svetlov, V., Loveland, A.B., Diaz-Avalos, R.,
595 Grigorieff, N., Nudler, E., and Korostelev, A.A. (2017). Structure of RNA polymerase
596 bound to ribosomal 30S subunit. Elife 6.

597 Drögemüller, J., Strauß, M., Schweimer, K., Jurk, M., Rösch, P., and Knauer, S.H.
598 (2015). Determination of RNA polymerase binding surfaces of transcription factors by
599 NMR spectroscopy. Sci Rep 5, 16428.

600 Dudenhoeffer, B.R., Schneider, H., Schweimer, K., and Knauer, S.H. (2019). SuhB is an

integral part of the ribosomal antitermination complex and interacts with NusA. Nucleic Acids Res. 47, 6504–6518.

Dutta, D., Shatalin, K., Epshtein, V., Gottesman, M.E., and Nudler, E. (2011). Linking RNA polymerase backtracking to genome instability in *E. coli*. Cell 146, 533–543.

Fan, H., Conn, A.B., Williams, P.B., Diggs, S., Hahm, J., Gamper, H.B., Hou, Y.-M., O'Leary, S.E., Wang, Y., and Blaha, G.M. (2017). Transcription-translation coupling: direct interactions of RNA polymerase with ribosomes and ribosomal subunits. Nucleic Acids Res. 45, 11043–11055.

Fu, J., Hashem, Y., Wower, I., Lei, J., Liao, H.Y., Zwieb, C., Wower, J., and Frank, J. (2010). Visualizing the transfer-messenger RNA as the ribosome resumes translation. EMBO J. 29, 3819–3825.

Grassucci, R.A., Taylor, D.J., and Frank, J. (2007). Preparation of macromolecular complexes for cryo-electron microscopy. Nat Protoc 2, 3239–3246.

Kang, J.Y., Mooney, R.A., Nedialkov, Y., Saba, J., Mishanina, T.V., Artsimovitch, I., Landick, R., and Darst, S.A. (2018). Structural Basis for Transcript Elongation Control by NusG Family Universal Regulators. Cell 173, 1650-1662.e14.

Knowlton, J.R., Bubunenko, M., Andrykovitch, M., Guo, W., Routzahn, K.M., Waugh, D.S., Court, D.L., and Ji, X. (2003). A spring-loaded state of NusG in its functional cycle is suggested by X-ray crystallography and supported by site-directed mutants. Biochemistry 42, 2275–2281.

621 Kohler, R., Mooney, R.A., Mills, D.J., Landick, R., and Cramer, P. (2017). Architecture
622 of a transcribing-translating expressome. Science 356, 194–197.

623 Krupp, F., Said, N., Huang, Y.-H., Loll, B., Bürger, J., Mielke, T., Spahn, C.M.T., and
624 Wahl, M.C. (2019). Structural Basis for the Action of an All-Purpose Transcription Anti-
625 termination Factor. Mol. Cell 74:143-157.

626 Kyrpides, N.C., Woese, C.R., and Ouzounis, C.A. (1996). KOW: a novel motif linking a
627 bacterial transcription factor with ribosomal proteins. Trends Biochem. Sci. 21, 425–426.

628 Langlois, R., Pallesen, J., Ash, J.T., Nam Ho, D., Rubinstein, J.L., and Frank, J. (2014).
629 Automated particle picking for low-contrast macromolecules in cryo-electron
630 microscopy. J. Struct. Biol. 186, 1–7.

631 Larson, M.H., Mooney, R.A., Peters, J.M., Windgassen, T., Nayak, D., Gross, C.A.,
632 Block, S.M., Greenleaf, W.J., Landick, R., and Weissman, J.S. (2014). A pause sequence
633 enriched at translation start sites drives transcription dynamics in vivo. Science 344,
634 1042–1047.

635 Lawson, M.R., Ma, W., Bellecourt, M.J., Artsimovitch, I., Martin, A., Landick, R.,
636 Schulten, K., and Berger, J.M. (2018). Mechanism for the regulated control of
637 transcription by a universal adapter protein. Mol. Cell 71, 1–12.

638 Livak, K.J., and Schmittgen, T.D. (2001). Analysis of relative gene expression data using
639 real-time quantitative PCR and the 2(-Delta Delta C(T)) Method. Methods 25, 402–408.

640 Luo, X., Hsiao, H.-H., Bubunenko, M., Weber, G., Court, D.L., Gottesman, M.E.,

641 Urlaub, H., and Wahl, M.C. (2008). Structural and functional analysis of the *E. coli*
642 NusB-S10 transcription antitermination complex. Mol. Cell 32, 791–802.

643 McGary, K., and Nudler, E. (2013). RNA polymerase and the ribosome: the close
644 relationship. Curr. Opin. Microbiol. 16, 112–117.

645 Mehdi, Q., and Yudkin, M.D. (1967). Coupling of transcription to translation in the
646 induced synthesis of beta-galactosidase. Biochim. Biophys. Acta 149, 288–290.

647 Meyer, O., and Schlegel, H.G. (1983). Biology of aerobic carbon monoxide-oxidizing
648 bacteria. Annu. Rev. Microbiol. 37, 277–310.

649 Miller, O.L., Hamkalo, B.A., and Thomas, C.A. (1970). Visualization of bacterial genes
650 in action. Science 169, 392–395.

651 Mitra, P., Ghosh, G., Hafeezunnisa, M., and Sen, R. (2017). Rho Protein: Roles and
652 Mechanisms. Annu. Rev. Microbiol. 71, 687–709.

653 Mooney, R.A., Schweimer, K., Rösch, P., Gottesman, M., and Landick, R. (2009a). Two
654 structurally independent domains of *E. coli* NusG create regulatory plasticity via distinct
655 interactions with RNA polymerase and regulators. J. Mol. Biol. 391, 341–358.

656 Mooney, R.A., Davis, S.E., Peters, J.M., Rowland, J.L., Ansari, A.Z., and Landick, R.
657 (2009b). Regulator trafficking on bacterial transcription units *in vivo*. Mol. Cell 33, 97–
658 108.

659 Newton, W.A., Beckwith, J.R., Zipser, D., and Brenner, S. (1965). Nonsense mutants and
660 polarity in the lac operon of *Escherichia coli*. J. Mol. Biol. 14, 290–296.

661 Pani, B., and Nudler, E. (2017). Mechanistic insights into transcription coupled DNA
662 repair. DNA Repair (Amst.) 56, 42–50.

663 Pettersen, E.F., Goddard, T.D., Huang, C.C., Couch, G.S., Greenblatt, D.M., Meng, E.C.,
664 and Ferrin, T.E. (2004). UCSF Chimera--a visualization system for exploratory research
665 and analysis. J Comput Chem 25, 1605–1612.

666 Phillips, J.C., Braun, R., Wang, W., Gumbart, J., Tajkhorshid, E., Villa, E., Chipot, C.,
667 Skeel, R.D., Kalé, L., and Schulten, K. (2005). Scalable molecular dynamics with
668 NAMD. J Comput Chem 26, 1781–1802.

669 Proshkin, S., Rahmouni, A.R., Mironov, A., and Nudler, E. (2010). Cooperation between
670 translating ribosomes and RNA polymerase in transcription elongation. Science 328,
671 504–508.

672 Rae, C.D., Gordiyenko, Y., and Ramakrishnan, V. (2019). How a circularized tmRNA
673 moves through the ribosome. Science 363, 740–744.

674 Roche, E.D., and Sauer, R.T. (1999). SsrA-mediated peptide tagging caused by rare
675 codons and tRNA scarcity. EMBO J. 18, 4579–4589.

676 Said, N., Krupp, F., Anedchenko, E., Santos, K.F., Dybkov, O., Huang, Y.-H., Lee, C.-T.,
677 Loll, B., Behrmann, E., Bürger, J., et al. (2017). Structural basis for λN-dependent
678 processive transcription antitermination. Nat Microbiol 2, 17062.

679 Sambrook, J., and Russel, D.W. (2001). Molecular Cloning: A Laboratory Manual (New
680 York: Cold Spring Harbor Press).

681 Saxena, S., Myka, K.K., Washburn, R., Costantino, N., Court, D.L., and Gottesman, M.E.
682 (2018). *Escherichia coli* transcription factor NusG binds to 70S ribosomes. Mol.
683 Microbiol. 108, 495–504.

684 Scheres, S.H.W. (2012). RELION: implementation of a Bayesian approach to cryo-EM
685 structure determination. J. Struct. Biol. 180, 519–530.

686 Sevostyanova, A., Belogurov, G.A., Mooney, R.A., Landick, R., and Artsimovitch, I.
687 (2011). The β subunit gate loop is required for RNA polymerase modification by RfaH
688 and NusG. Mol. Cell 43, 253–262.

689 Sharan, S.K., Thomason, L.C., Kuznetsov, S.G., and Court, D.L. (2009).
690 Recombineering: a homologous recombination-based method of genetic engineering. Nat
691 Protoc 4, 206–223.

692 Squires, C.L., Greenblatt, J., Li, J., Condon, C., and Squires, C.L. (1993). Ribosomal
693 RNA antitermination in vitro: requirement for Nus factors and one or more unidentified
694 cellular components. Proc. Natl. Acad. Sci. U.S.A. 90, 970–974.

695 Suloway, C., Pulokas, J., Fellmann, D., Cheng, A., Guerra, F., Quispe, J., Stagg, S.,
696 Potter, C.S., and Carragher, B. (2005). Automated molecular microscopy: the new
697 Leginon system. J. Struct. Biol. 151, 41–60.

698 Thommen, M., Holtkamp, W., and Rodnina, M.V. (2017). Co-translational protein
699 folding: progress and methods. Curr. Opin. Struct. Biol. 42, 83–89.

700 Trabuco, L.G., Villa, E., Mitra, K., Frank, J., and Schulten, K. (2008). Flexible fitting of

atomic structures into electron microscopy maps using molecular dynamics. Structure 16, 673–683.

Vogel, U., and Jensen, K.F. (1994). Effects of guanosine 3',5'-bisdiphosphate (ppGpp) on rate of transcription elongation in isoleucine-starved *Escherichia coli*. J. Biol. Chem. 269, 16236–16241.

Vogel, U., and Jensen, K.F. (1995). Effects of the antiterminator *BoxA* on transcription elongation kinetics and ppGpp inhibition of transcription elongation in *Escherichia coli*. J. Biol. Chem. 270, 18335–18340.

Vvedenskaya, I.O., Vahedian-Movahed, H., Bird, J.G., Knoblauch, J.G., Goldman, S.R., Zhang, Y., Ebright, R.H., and Nickels, B.E. (2014). Interactions between RNA polymerase and the "core recognition element" counteract pausing. Science 344, 1285–1289.

Washburn, R.S., and Gottesman, M.E. (2011). Transcription termination maintains chromosome integrity. Proc. Natl. Acad. Sci. U.S.A. 108, 792–797.

Weis, F., Bron, P., Giudice, E., Rolland, J.-P., Thomas, D., Felden, B., and Gillet, R. (2010). tmRNA-SmpB: a journey to the centre of the bacterial ribosome. EMBO J. 29, 3810–3818.

Werner, F. (2012). A nexus for gene expression-molecular mechanisms of Spt5 and NusG in the three domains of life. J. Mol. Biol. 417, 13–27.

Zhang, X., and Bremer, H. (1995). Control of the *Escherichia coli rrnB* P1 promoter

721 strength by ppGpp. J. Biol. Chem. 270, 11181–11189.

722 Zuber, P.K., Artsimovitch, I., NandyMazumdar, M., Liu, Z., Nedialkov, Y., Schweimer,
723 K., Rösch, P., and Knauer, S.H. (2018). The universally-conserved transcription factor
724 RfaH is recruited to a hairpin structure of the non-template DNA strand. Elife 7.

725 Zuber, P.K., Schweimer, K., Rösch, P., Artsimovitch, I., and Knauer, S.H. (2019).
726 Reversible fold-switching controls the functional cycle of the antitermination factor
727 RfaH. Nat Commun 10, 702.

728

729

730

731 **Figures**

732

733

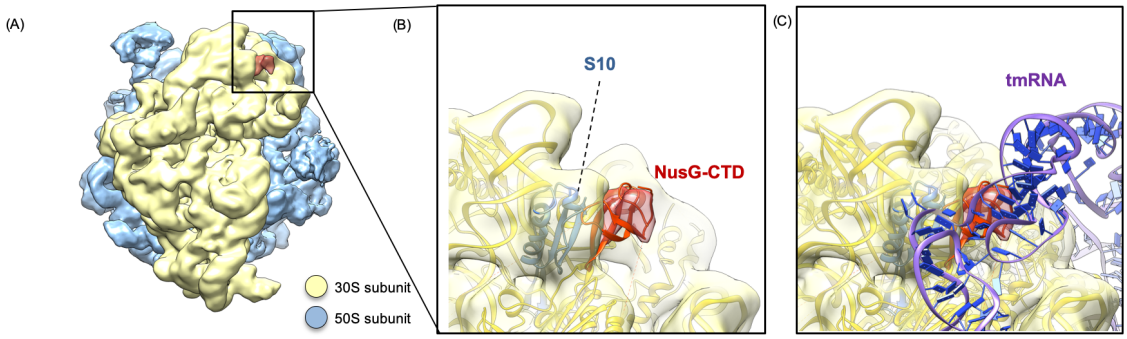

734

735 **Figure 1. Structure of NusG-CTD bound to 70S ribosome. (A)** Cryo-EM density of
736 the 70S ribosome:NusG complex. The density of the 50S subunit is shown in light blue,
737 the density of the 30S subunit in yellow, the density corresponding to NusG-CTD in red.
738 **(B)** Close-up view of the region boxed in **(A)**. 70S (yellow), S10 (blue), and NusG-CTD
739 (red) are in ribbon representation, cryo-EM density is shown as transparencies. **(C)**
740 Superposition of the 70S:NusG complex with the 70S:tmRNA complex (tmRNA is in
741 ribbon representation, purple and dark blue; EMD 5234, PDB: 3IZ4). 30S and NusG-
742 CTD are displayed as in **(B)**.

743

744

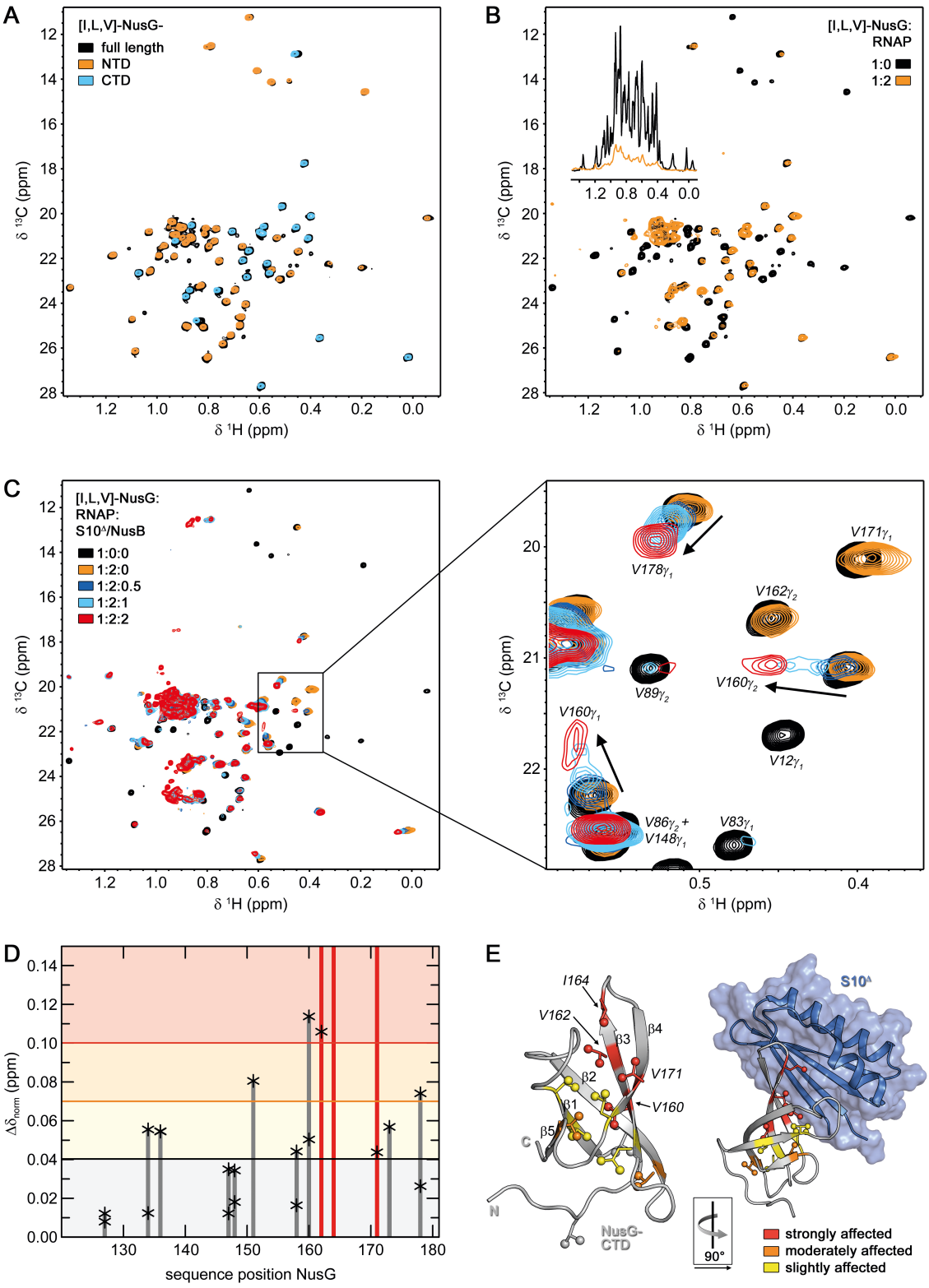

Figure 2. RNAP-bound NusG interacts with S10. (A) Superposition of 2D [^{1}H, ^{13}C]-methyl-TROSY spectra of [ILV]-NusG (black, 20 μM), [ILV]-NusG-NTD (orange, 100

748 µM), and [ILV]-NusG-CTD (cyan, 30 µM). **(B)** 2D [^{1}H, ^{13}C]-methyl-TROSY spectra of
749 [ILV]-NusG in the absence (black, 20 µM) and presence (orange, 18 µM) of two
750 equivalents of RNAP. Inset: Normalized 1D [^{1}H,^{13}C]-methyl TROSY spectra, colored as
751 2D spectra. **(C)** 2D [^{1}H, ^{13}C]-methyl-TROSY spectra of [ILV]-NusG alone (20 µM), in
752 the presence of a twofold molar excess of RNAP (18 µM [ILV]-NusG), and upon
753 titration of [ILV]-NusG:RNAP with 218 µM S10$^{\lambda}$:NusB. The molar ratio of [ILV]-
754 NusG:RNAP:S10$^{\lambda}$:NusB is indicated in color. The panel on the right shows an
755 enlargement of the boxed region. Selected signals are labeled and arrows indicate
756 chemical shift changes upon S10$^{\lambda}$:NusB addition. **(D)** [^{1}H,^{13}C]-methyl-TROSY-derived
757 normalized chemical shift changes of [ILV]-NusG-CTD methyl group signals of RNAP-
758 bound [ILV]-NusG upon complex formation with S10$^{\lambda}$:NusB. Asterisks mark the values
759 of individual methyl group signals, bars represent the highest values. Red bars indicate
760 vanishing signals. Horizontal lines are thresholds for affected methyl groups: slightly
761 affected (0.04 ppm ≤ $\Delta\delta_{norm}$ < 0.07 ppm; black), moderately affected (0.07 ppm ≤ $\Delta\delta_{norm}$
762 < 0.1 ppm; orange), and strongly affected ($\Delta\delta_{norm}$ ≥ 0.10 ppm; red). **(E)** Mapping of
763 affected methyl groups on the structure of isolated NusG-CTD (left; PDB ID: 2JVV) and
764 NusG-CTD in complex with S10$^{\lambda}$ (right; PDB ID 2KVQ). NusG-CTD is shown in ribbon
765 (gray), S10$^{\lambda}$ in ribbon and surface (blue) representation. Affected Ile, Leu, and Val
766 residues are colored according to **(D),** non-affected Ile, Leu, and Val residues are gray.
767 Side chains of Ile, Leu, and Val residues are depicted as sticks, their methyl groups as
768 spheres. Strongly affected Ile, Leu, and Val residues are labeled. The orientation of
769 NusG-CTD in the complex relative to the isolated state is indicated.
770

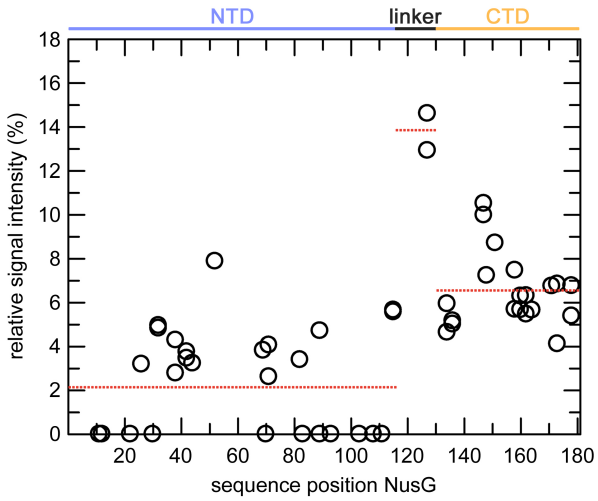

Figure 2-figure supplement 1: Binding of [ILV]-NusG to RNAP. [^{1}H,^{13}C]-methyl-TROSY derived relative signal intensities of [ILV]-NusG methyl groups after addition of two equivalents of RNAP (see Fig. 2B). Red, dashed horizontal lines indicate average relative signal intensities of NusG-NTD, the linker, and NusG-CTD (domain organization is indicated at the top). Related to Figure 2B.

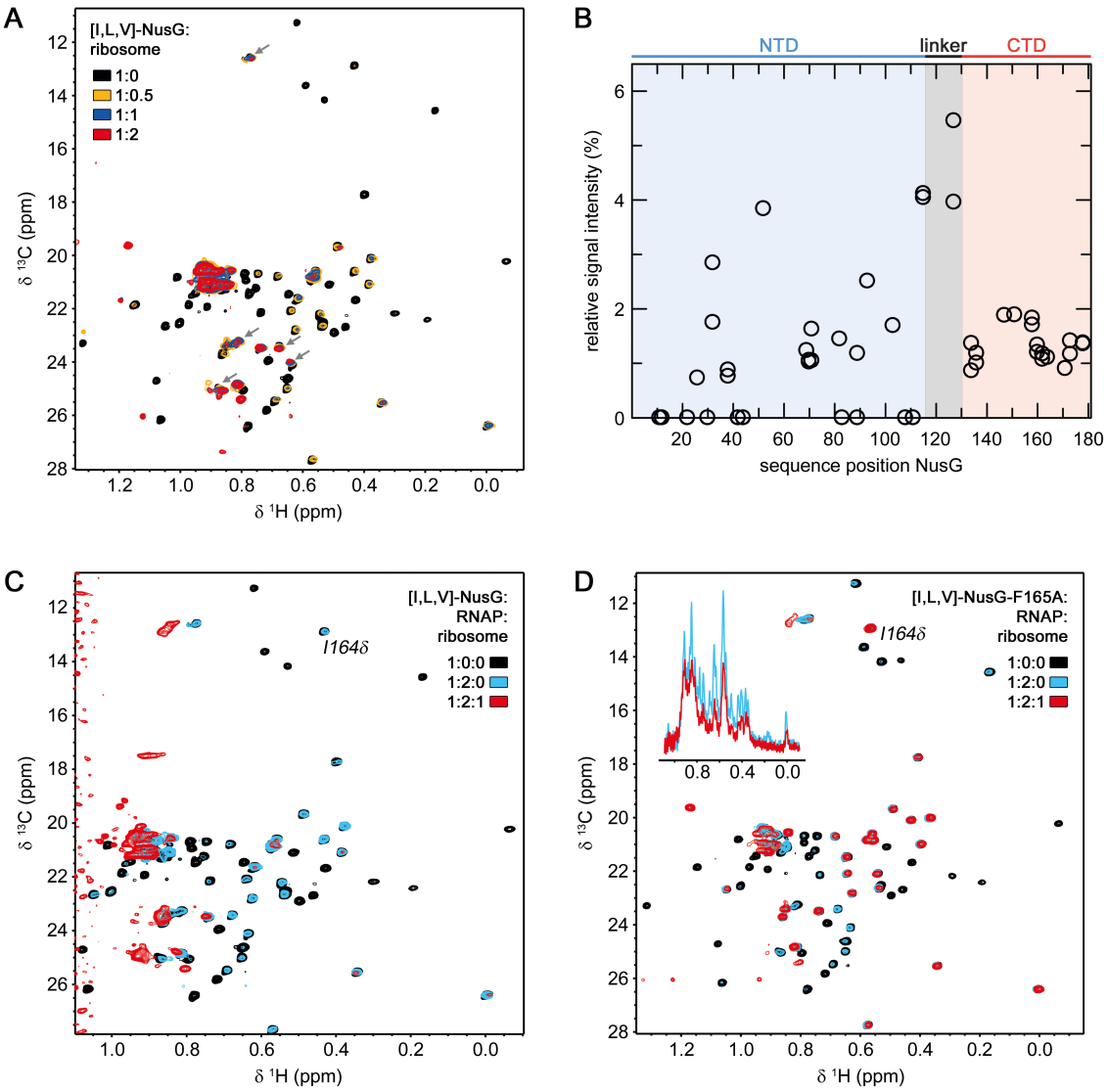

Figure 3: RNAP-bound NusG interacts with the 70 S ribosome. (A,B) NusG interacts with 70S ribosome via its CTD. **(A)** 2D [^{1}H, ^{13}C]-methyl-TROSY spectra of free [ILV]-NusG (11 µM, black) and [ILV]-NusG in the presence of 70S ribosome (molar ratio [ILV]-NusG:ribosome = 1:0.5 (6.6 µM [ILV]-NusG, orange); = 1:1 (7.5 µM [ILV]-NusG, blue); =1:2 (4 µM [ILV]-NusG, red). Arrows indicate [ILV]-NusG-NTD signals that are well visible in the [ILV]-NusG:ribosome complex. **(B)** Quantitative analysis of [ILV]-NusG methyl group signal intensities in the presence of 0.5 equivalents of 70S ribosome. Relative signal intensities are plotted versus the sequence position of NusG.

787 The domain organization of NusG is indicated above the diagram. **(C)** 2D [^{1}H, ^{13}C]-
788 methyl-TROSY spectra of [ILV]-NusG (11 μM, black), [ILV]-NusG in the presence of
789 RNAP (molar ratio 1:2, 6 μM [ILV]-NusG, blue), and [ILV]-NusG in the presence of
790 RNAP and 70S ribosome (molar ratio 1:2:1, 6 μM [ILV]-NusG, red). **(D)** 2D [^{1}H, ^{13}C]-
791 methyl-TROSY spectra of [ILV]-NusG^{F165A} (20 μM, black), [ILV]-NusG^{F165A} in the
792 presence of RNAP (molar ratio 1:2, 6 μM [ILV]-NusG^{F165A}, blue), and [ILV]-NusG^{F165A}
793 in the presence of RNAP and 70S ribosome (molar ratio 1:2:1, 6 μM [ILV]-NusG^{F165A},
794 red). The inset shows the normalized 1D spectra of the corresponding titration step.
795

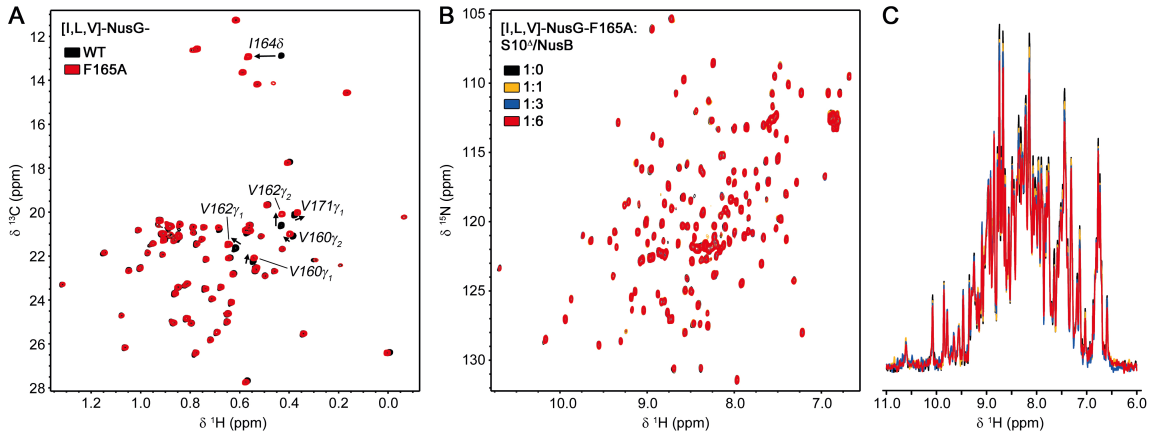

Figure 3-figure supplement 1: NusG-F165A does not interact with S10^{A}/NusB. (A) 2D [^{1}H, ^{13}C]-methyl-TROSY spectra of [ILV]-NusG (11 µM, black) and [ILV]-NusG^{F165A} (20 µM, red). Arrows and labels indicate NusG-CTD methyl groups affected in their resonance frequencies by the F165A amino acid substitution. **(B,C)** 2D **(B)** and normalized 1D **(C)** [^{1}H, ^{15}N]-HSQC spectra of 20 µM [ILV]-NusG^{F165A} upon titration with 432 µM S10^{A}/NusB (colors as indicated).

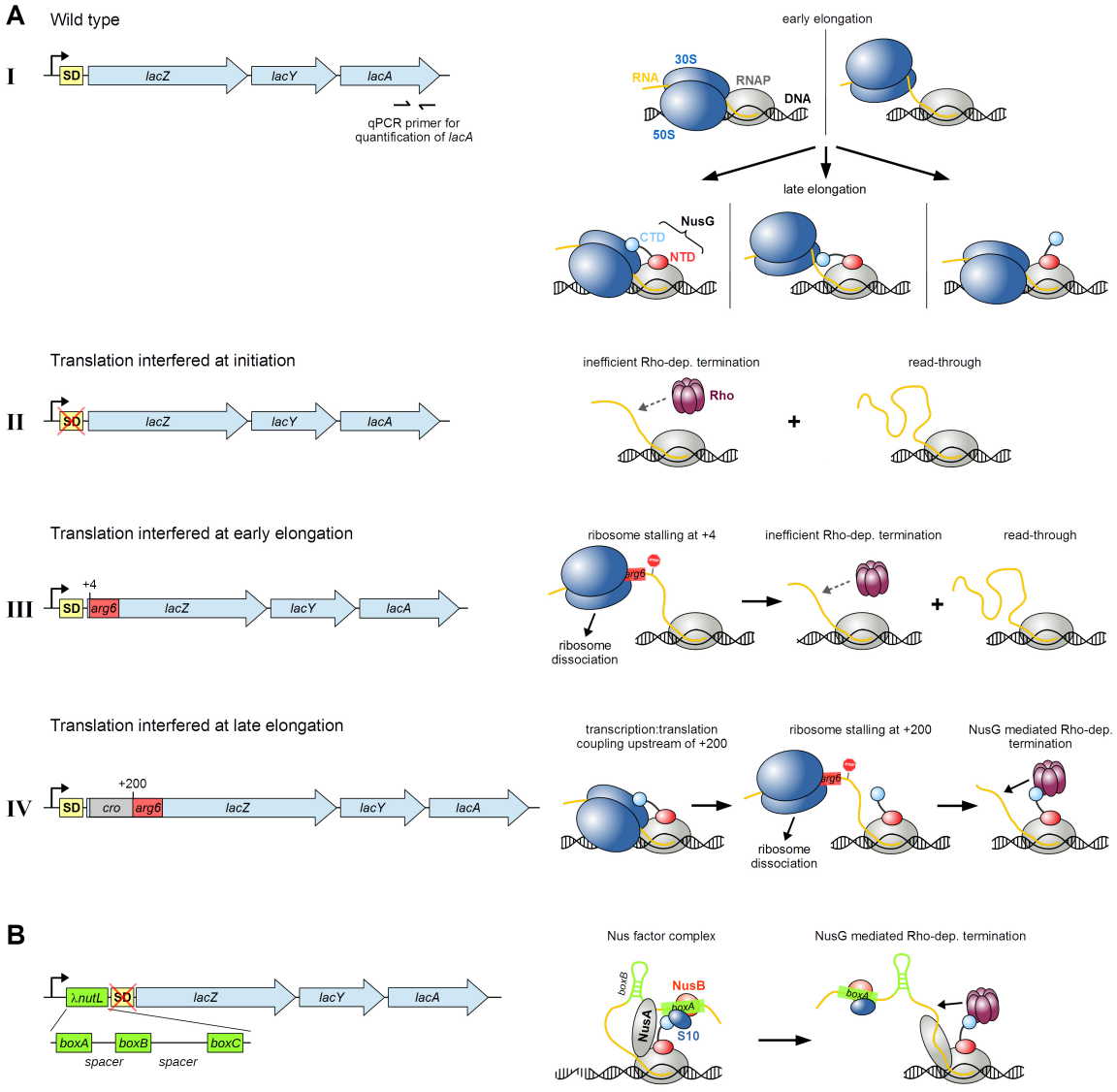

806

807 **Figure 4: Translation is required for NusG recruitment to the TEC. (A, B)** Left:
808 Organization of the *E. coli lac* operon in strains MDS42 (A-I; wild type *lacZ*), RSW1225
809 (A-II; mutant (inactive) *lacZ* SD sequence), RSW1245 (A-III; in-frame insertion of six
810 rare Arg codons (*arg6*) at position +4 of *lacZ*), RSW1276 (A-IV; in-frame insertion of
811 λ*cro* and six rare Arg codons at position +4 of *lacZ* (equivalent to *arg6* being at position
812 +200 of the gene)), and RSW1297 (B; λ*nutL* site upstream of mutant *lacZ* SD sequence).
813 SD sequences of *lacY* and *lacA* were omitted for clarity. qPCR primers specific to the 3'
814 end of *lacA* (position indicated in A-I) were used to measure mRNA levels and thereby

read-through of *lacA* (see Table 1). Right: Schemes of possible effects on transcription:translation coupling and Rho-dependent termination within *lacZ*. A-I, top: Ribosomes are recruited in the early elongation phase, leading to a directly coupled RNAP:ribosome complex (left) or uncoupled transcription and translation (right). A-I, bottom: NusG is recruited in late elongation, resulting in a NusG-coupled complex with (left) or without direct RNAP:ribosome contacts (middle), or modifying the pre-existing RNAP:ribosome complex without establishing an CTD:S10 interaction (right). A-II: Failure of NusG recruitment results in inefficient Rho-dependent termination and high *lacA* read-through. A-III: *arg6* stops the translating ribosome at position +4, whereas transcription elongation proceeds (left), resulting in ribosome dissociation and no NusG recruitment. Transcription proceeds and is only inefficiently terminated by Rho (right). A-IV: NusG couples transcription and translation (left) until *arg6* stops the ribosome at position +200 (middle), allowing efficient, NusG-stimulated Rho-dependent termination (right). B: λ*nutL* recruits NusA, NusG and the S10/NusB dimer, creating a Nus complex (left). NusG can thus support Rho-dependent termination.

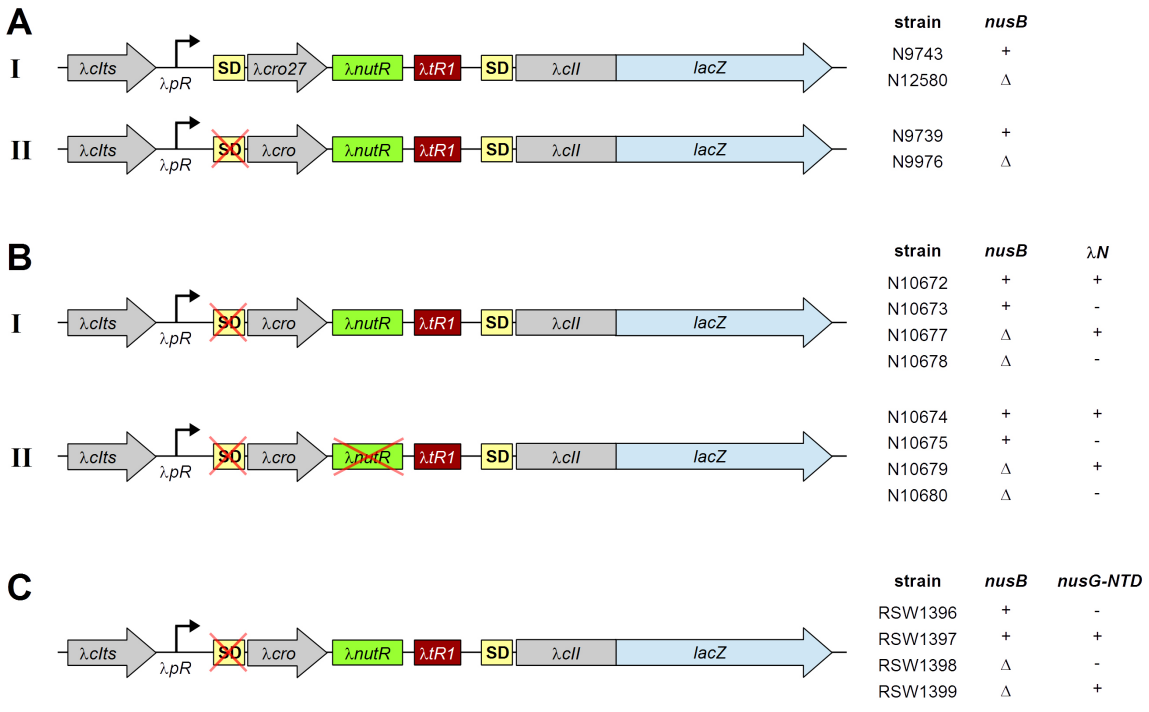

Figure 5: NusG can be recruited *via* a Nus complex. Genetic constructs used to monitor NusG mediated Rho-dependent termination are shown with the corresponding strains and their properties indicated on the right side. Transcription is started from the λ*pR* promoter, followed by WT-λ*cro* or λ*cro* carrying a missense mutation at codon 27 (λ*cro27*), a WT or mutant λ*nutR* site (B), the Rho-dependent terminator λ*tR1* and a λ*cII::lacZ* transcriptional fusion with corresponding SD site. All strains encode a temperature sensitive λcI construct (λ*cIts*) to allow temperature-controlled induction of gene expression from the λ*pR* promoter. λN^{+} strains listed in (B) further encode the λN protein; NusG-NTD for strains listed in (C) was supplied from plasmid pRM442. See also tables 2A-C.

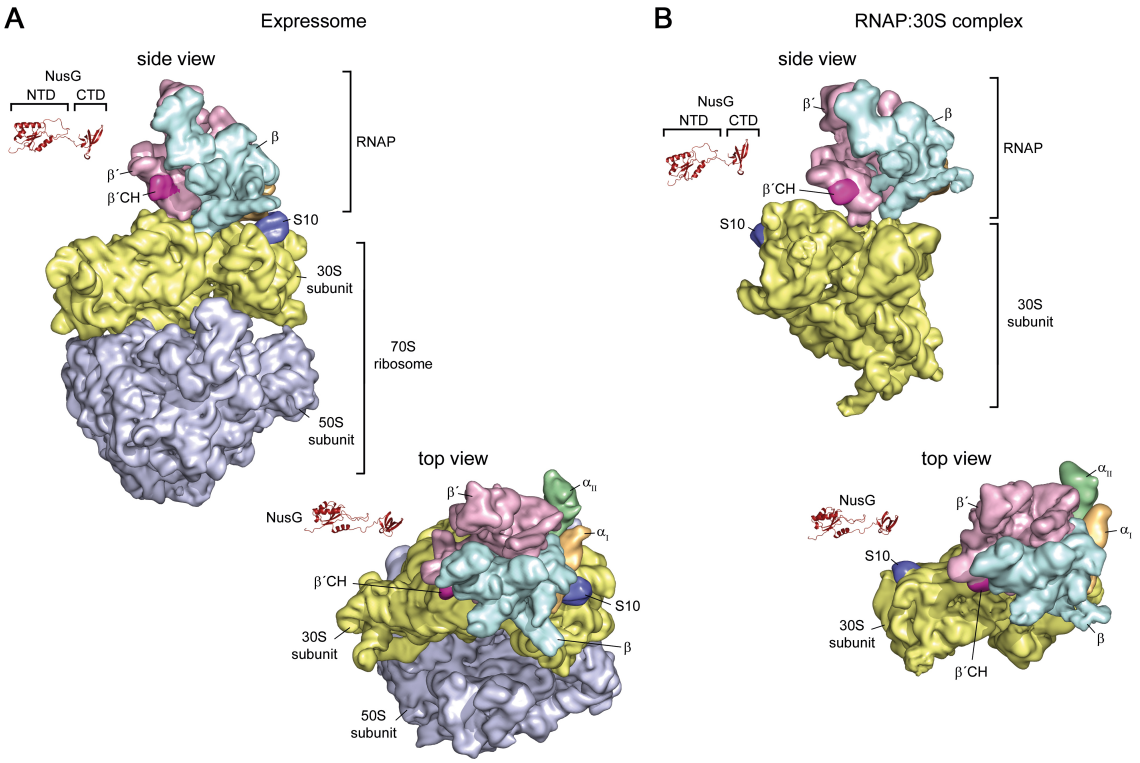

844

845 **Figure 6: Structures of coupling complexes.** Structures of the expressome (A) and an
846 RNAP:30S complex (B) determined by cryo-EM are shown. RNAP and ribosomal
847 subunits are in surface representation, NusG is shown as ribbon. α_I, orange; α_{II} green; β,
848 cyan; β', light violet; 30S, yellow; 50S, light blue; β'CH, pink; S10, dark blue. PDB IDs:
849 expressome, 5MY1 and 6O9J; RNAP:30S, 6AWD; NusG-NTD: 2K06; NusG-CTD:
850 2JVV

851

852

853 **Tables**

854

855 **Table 1. NusG couples late after transcription initiation.** β-galactosidase was induced
856 for 20 min from the *lac* operon with1mM IPTG. Where indicated, Rho-dependent
857 termination was inhibited by adding 100μg/ml BCM 1 minute prior to induction. Read-
858 through was calculated from the fold-increase of *lacA RNA* compared to *ompA* RNA in
859 the presence or absence of BCM. RNA levels were measured using qRT-PCR and the
860 fold- increase calculated using the $\Delta\Delta C_t$ method (Livak and Schmittgen, 2001).
861 RSW1225 carries two G to A mutations in the *lacZ* ribosome-binding site. RSW1245
862 carries an insertion of six rare arginine codons (atg-acc-atg-AGG-AGA-CGA-AGG-
863 AGA-CGA) at the amino terminus of *lacZ*. RSW1276 contains six rare arginine codons
864 200nt distal to the start of translation. RSW1297 carries an insertion of λ*nutL*
865 immediately 5' to the mutated ribosome binding site.

strain	***lacZ***	***nutL***	**BCM$^-$**	**BCM$^+$**	**RT (%)**
MDS42	wt	-	.25	.26	99
RSW1225	SD$^-$	-	.12	.56	21
RSW1245	arg(6) - early	-	.13	.49	29
RSW1276	arg(6) - late	-	<.01	.12	<1
RSW1297	SD$^-$	+	.01	.59	1

866

Table 2. NusG recruitment depends on translation. (A) NusG coupling at *nutR* requires NusB. Expression of β-galactosidase was induced from a chromosomal *cII*::lacZ transcriptional fusion (λ*cIts-pR-cro-nutR-tR1-cII::lacZ*) by incubating at 42^0 C for 30 min. N9743 and N12580 carry a missense mutation at *cro* codon 27, N9739 and 9976 have a G to C mutation in the *cro* Shine Dalgarno sequence (*SD*-), N12580 and N9976 are deleted for *nusB*. Where indicated, bicyclomycin (BCM) was added to 100μg/ml prior to induction of β-galactosidase. Read-through (RT) was calculated from the ratio of β-galactosidase activity in the presence or absence of BCM. **(B)** BoxA mutations block NusG coupling at *nutR*. Expression of β-galactosidase was induced from a chromosomal *cII*::lacZ transcriptional fusion (λ*cIts-pR-cro* (*SD*$^-$) *-nutR-tR1-cII::lacZ*) by incubating at 42^0 C for 30 min. Strains N10672, N10674, N10677 and N10679 express the λN transcription termination inhibitor. *boxA69* and Δ*nusB* strain numbers are indicated in Table 3. Read-through (RT) was calculated from the ratio of β-galactosidase activity in the presence or absence of λN. **(C)** NusG-NTD uncouples. Expression of β-galactosidase was induced from a chromosomal *cII*::lacZ transcriptional fusion (λ*cIts-pR-cro(*SD$^-$*)-nutR-tR1-cII::lacZ*) by incubating at 42^0 C for 30 min. The NusG-NTD was induced from the plasmid pRM442 *tac* promoter with 1mM IPTG for 10 min prior to induction of β−galactosidase in strains RSW1397 and RSW 1399. Strains RSW1396 and RSW1398 carried an empty vector (p*trc99A*) and were exposed to IPTG as above. Where indicated bicyclomycin (BCM) was added to 100μg/ml prior to induction of β-galactosidase. Read-through (RT) was calculated from the ratio of β-galactosidase activity in the presence or absence of BCM.

889

A	**strain**	***cro***	***nusB***	**BCM$^-$**	**BCM$^+$**	**RT (%)**
	9743	*ms27*	+	530	680	78
	12580	*ms27*	D	890	1150	78
	9739	SD-	+	141	613	**23**
	9976	SD-	D	1191	1290	92

890

B	**strain**	***boxA***	***nusB***	**λN$^-$**	**λN$^+$**	**RT (%)**
	10673, 10672	+	+	126	946	**13**
	10675, 10674	*69*	+	1212	2211	55
	10678, 10677	+	D	2874	2616	100
	10680, 10679	*69*	D	1896	2416	78

891

C	**strain**	***nusG-NTD***	***nusB***	**BCM$^-$**	**BCM$^+$**	**RT (%)**
	RSW1396	-	+	247	862	**29**
	RSW1397	+	+	944	1013	93

	RSW1398	–	Δ	2013	2314	93
	RSW1399	+	Δ	2360	2760	86

892

893

894